A highly efficient antibacterial solar-thermal evaporator based on waste tea leaves for water evaporation and thermoelectric generation

Yijun Zhao,[a] Fei Wang,[a] Zuoyu Wang,[a] Yingyuan Zhang,[a] Nanxi Jin,*[c] Tao Jia,*[a,b] Xiuhua Zhao[a,b]

a. Key Laboratory of Forest Plant Ecology, Ministry of Education, Engineering Research Center of Forest Bio-Preparation, College of Chemistry, Chemical Engineering and Resource Utilization, Northeast Forestry University, Harbin 150040, P. R. China.

b. State Key Laboratory of Utilization of Woody Oil Resource, Northeast Forestry University, Harbin 150040, P. R. China.

c. Department of Biomedical Statistics, Graduate School of Medicine and Integrated Frontier Research for Medical Science Division, Osaka University, Osaka, Japan.

*Corresponding author. E-mail: jiataopolychem@nefu.edu.cn (Tao Jia); u985821a@ecs.osaka-u.ac.jp (Nanxi Jin)

General information: The UV-vis-NIR absorption spectra of waste Maojian tea (WMT) powder and hydrogel samples were recorded by the Shimadzu UV-2550 spectrophotometer. The morphology of the solar-thermal evaporator was observed by scanning electron microscopy (SEM, EM-30plus). The infrared absorption spectra of WMT were measured by Fourier transform infrared spectrometer (Nicolet IS10). Freeze-drying was performed by the vacuum freeze dryer FD-1A-50+. The contact angle was measured by the Contact Angle tester 14004485 DSA-100S. Ion concentration after seawater desalination was tested by avio 200 inductively coupled plasma emission spectrometer. Sterilization was performed by vertical sterilizer LS-28HD. The antibacterial experiment was conducted in the ultra-clean workbench. The bacterial morphology was observed by Ultra-high resolution field emission scanning electron microscope (Apreo 2 SEM). The solid culture medium was cultivated in a constant temperature and humidity incubator YRH-800.

Solar-thermal experiments: Infrared thermal imager (TESTO-869) was used to record the change of temperature. Water evaporation and thermoelectric generation were carried out with xenon Cell-S500/350 light source (AM 1.5 G spectral filter) was used as a thermoelectric device, and FLUKE 8846A system was used to obtain the open circuit voltage data. The thermal stability of WMT is measured by a thermogravimetric analyzer (TGA8000).

Solar steam generation experiments: Polystyrene foam supported the WMT/H, with a hollowed-out center keeping the WMT/H in constant contact with water at its bottom. Sunlight was generated by a solar simulator with a standard AM 1.5 G spectrum (CEL-S500/350) filter, and irradiated the sample under specific optical concentrations. The weight loss of water was measured by an analytical balance and the temperature of entire process was recorded by an infrared thermal imager. The energy conversion efficiency was measured.

Solar temperature difference power generation: Commercial thermoelectric generator (TES1-24103-SR, length 40 mm, width 40 mm, height 3.6 mm) was selected for power generation. By integrating WMT with a commercial thermoelectric power generation device (TES1-24103-SR), a solar-thermal-electricity combined production device was formed. The WMT solar absorber was placed on the top surface as the hot side, and on the bottom surface it was placed on the cooling unit, with circulating condensed water serving as the cold side. Subsequently, power generation tests were conducted at power levels of 1 kW m^{-2} for the long-term (6 h), and the surface temperature was captured and recorded by an infrared thermal imager. For water-electricity combined production device, the thermoelectric sheet (TES1-24103-SR) was supported by polystyrene foam, covered with WMT/H on top, and in contact with the water surface below. Water-electricity cogeneration open circuit voltage (V_{OC}) were measured and recorded by Keithley 6514 system electrometer instrument. Subsequent power generation experiments were conducted at the 1, 2, and 5 kW m^{-2}, and the surface temperature was captured and recorded by an infrared thermal imager.

Calculation of the solar-thermal conversion efficiency: The solar-thermal conversion efficiency (η) was calculated as the following formula:

$$\eta = \frac{Q}{E} = \frac{Q_1 - Q_2}{E}$$

Where Q refers to the thermal energy generated (i.e., $Q = Q_1 - Q_2$), Q_1 is the thermal energy generated of WMT and Q_2 is the thermal energy generated of pure water. E refers to the total energy of the incident light. Q is determined by the heat capacity (C), density (ρ), volume (V) and ΔT over the period of irradiation of the solution; E is determined by the power (P) of the incident light, the irradiation area (S) and irradiation time (t). Therefore, the specific formula is as follows:

$$Q_1 = Cm\Delta T_1 = C\rho V\Delta T_1$$

$$Q_2 = Cm\Delta T_2 = C\rho V\Delta T_2$$

$$E = PSt$$

In this work, since samples are present in very low amounts in the solution, values of C (4.2 J g^{-1} $°C^{-1}$) and ρ (1 g cm^{-3}) for water were used in the calculations. For example, the surface temperature of WMT powder was 44.0 ℃ during the irradiation process, and the initial temperature is 22.3 ℃, therefore ΔT is 21.7 ℃. As the above formulas.

$Q_1 = C\rho V\Delta T_1 = 4.2 \times 1 \times 1 \times (44.0-22.3) = 91.14\ J$

$Q_2 = C\rho V\Delta T_2 = 4.2 \times 1 \times 1 \times (38.9-21.6) = 72.66\ J$

$E = PSt = 0.1 \times 1.5386 \times 1200 = 184.632\ W \cdot s$

$$\eta = \frac{Q_1-Q_2}{E} = \frac{91.14-72.66}{184.632} = 10.01\%$$

As a result, WMT solar-thermal conversion efficiency η = (Q_1-Q_2)/E =10.01% when the temperature difference is 21.7 ℃ is calculated.

Calculation of the efficiency for solar to vapor generation: The conversion efficiency η of solar energy in solar-thermal assisted water evaporation was calculated as the following formula.

$$\eta = \frac{\dot{m}h_{LV}}{C_{opt}P_0}$$

Where ṁ refers to the mass flux (evaporation rate) of water (i.e., $\dot{m} = m_{solar} - m_{dark}$), m_{solar} is the evaporation rate under solar irradiation and m_{dark} is the evaporation rate under dark circumstance, h_{LV} refers to the total liquid vapor phase-change enthalpy (i.e., the sensible heat and the enthalpy of vaporization (i.e., $h_{LV} = Q + \Delta h_{vap}$)), Q is the energy provided to heat the system from the initial temperature to a final temperature, Δh_{vap} is the latent heat of vaporization of water. P_0 is the nominal solar irradiation value of 1.0 kW m^{-2}, and C_{opt} represents the optical concentration. The schematic for the vaporization enthalpy of the vapor was as follows.

$Q = C_{liquid} \times (T-T_0)$

$\Delta h_{vap} = \Delta h_{40.2}$

$$\ln(\frac{P_2}{P_1}) = -\frac{\Delta h_{40.2}}{R}(\frac{1}{T_2}-\frac{1}{T_1})$$

In this work, C_{liquid}, the specific heat capacity of liquid water is a constant of 4.18 J (g ^{o}C)$^{-1}$. C_{vapor}, the specific heat capacity of water vapor is a constant of 1.865 J (g ^{o}C)$^{-1}$. $\Delta h_{40.2}$ is the latent heat of vaporization of water at 40.2 ^{o}C, which is calculated using the Clausius-Clapeyron equation. P_1 and P_2 represent the saturated vapor pressures of 100 ℃ and 40.2 ℃ respectively. T_1 and T_2 represent the absolute temperature in the Kelvin scale (K). R represents the ideal gas constant, which is set to 8.314 J·mol^{-1}·K^{-1}. It can be obtained from the standard physical chemistry data that P_2 is 7.52 kPa and P_1 is 101.325 kPa. After calculation, we obtain T_2 = 40.2 + 273.15 = 313.35 K, and T_1 = 100.0 + 273.15 = 373.15 K. The surface temperature of the WMT/H was 40.2 ^{o}C during the evaporation process, therefore T is 40.2 ^{o}C. As the above formulas,

$$Q = C_{liquid} \times (T - T_0) = 4.18 \times (40.2 - 19.0) = 88.616\ kJ\ kg^{-1}$$

$$\Delta h_{vap} = \Delta h_{40.2} = 2346.741\ kJ\ kg^{-1}$$

$$h_{LV} = Q + \Delta h_{vap} = 88.616 + 2346.741 = 2435.357\ kJ\ kg^{-1}$$

$$m_{solar} = 1.3587\ kg\ m^{-2}\ h^{-1}$$

$$m_{dark} = 0.2313\ kg\ m^{-2}\ h^{-1}$$

$$\dot{m} = m_{solar} - m_{dark} = 1.1274\ kg\ m^{-2}\ h^{-1}$$

$$P_0 = 1000\ W\ m^{-2}$$

$$C_{opt} = 1$$

As a result, water evaporation rate is 1.36 kg m^{-2} h^{-1}, evaporation efficiency $\eta = \dot{m}h_{LV}/C_{opt}P_0$ = 76.28% when the latent heat of water vaporization at 40.2 ^{o}C (2435.357 kJ kg^{-1}) is used in calculation.

Supplementary figures:

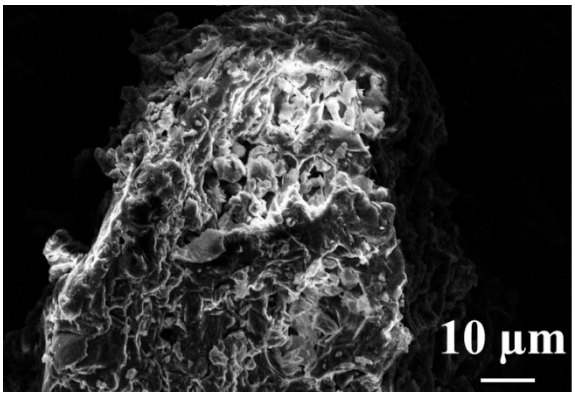

Figure S1. SEM image of WMT powder.

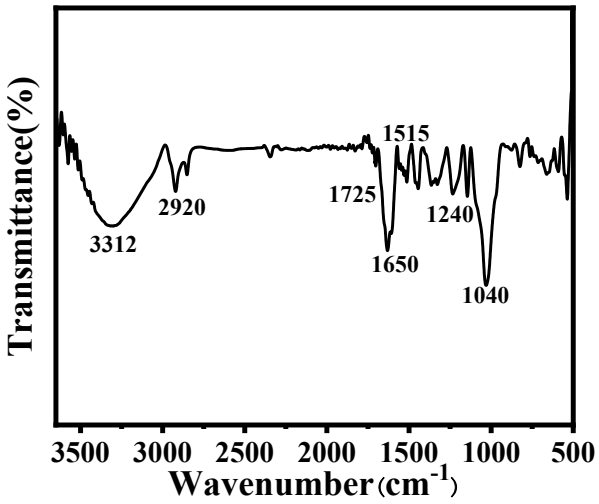

Figure S2. Infrared spectra of WMT powder.

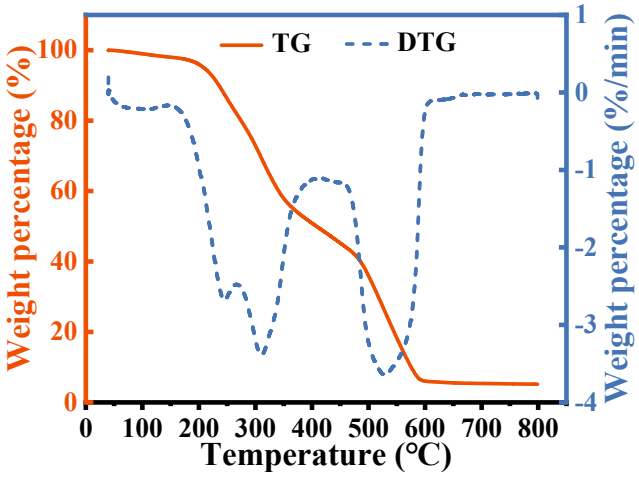

Figure S3. TG and DTG curves of WMT powder.

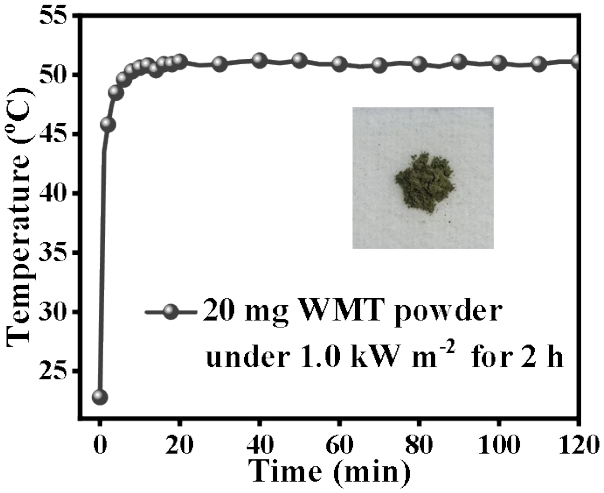

Figure S4. Temperature changes of WMT powder under 2 h irradiation under 1.0 kW m^{-2} irradiation.

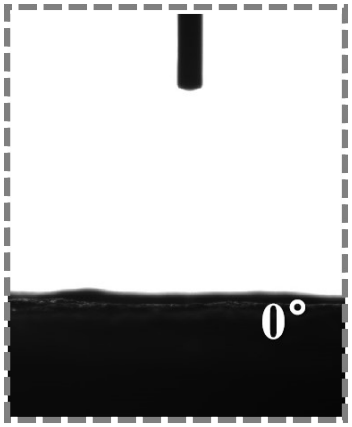

Figure S5. Digital photographs of contact angles of water droplets on the WMT/H surface.

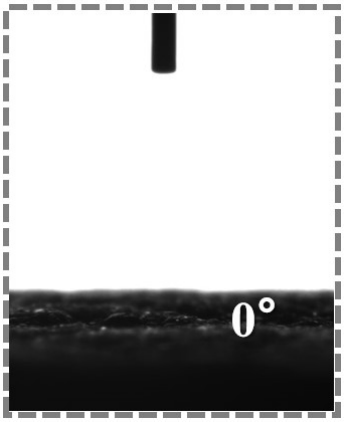

Figure S6. Digital photographs of contact angles of water droplets on the blank hydrogel surface.

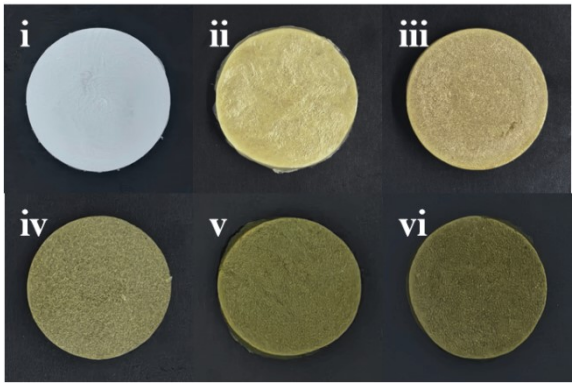

Figure S7. Digital photographs of WMT/H at different concentrations.

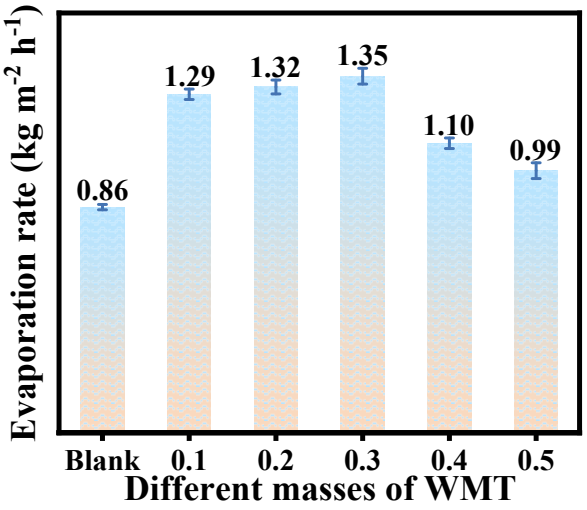

Figure S8. Evaporation rate of water from WMT/H prepared from WMT powder of different masses.

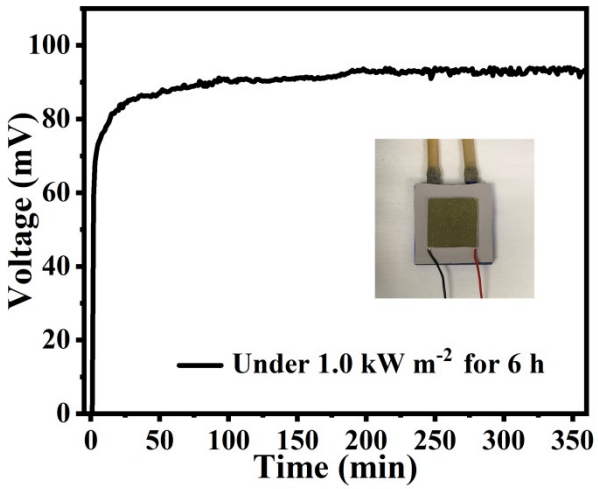

Figure S9. Long-term durability curve of thermal-electric devices.

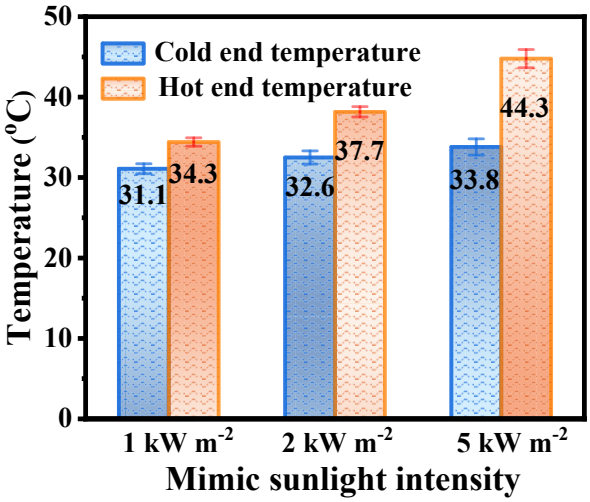

Figure S10. Comparison of temperature between WMT/H and water after 3 min of irradiation under different solar densities.

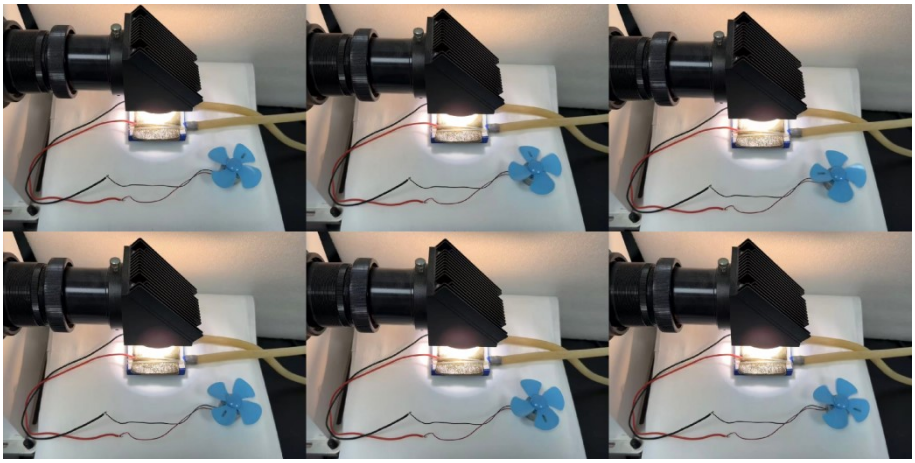

Figure S11. Digital photograph of small fan-driven by WMT/H power generation system.

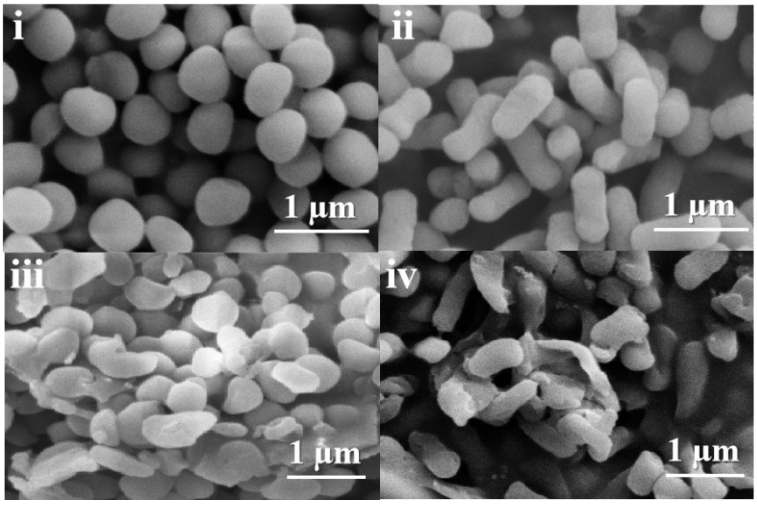

Figure S12. SEM image of bacterial morphology (i and iii represent the

morphological changes of *Staphylococcus aureus* before and after the antibacterial experiment; ii and iv represent the morphological changes of *Escherichia coli* before and after the antibacterial experiment).

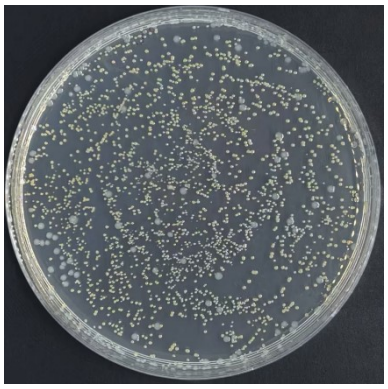

Figure S13. The growth of bacteria in seawater.

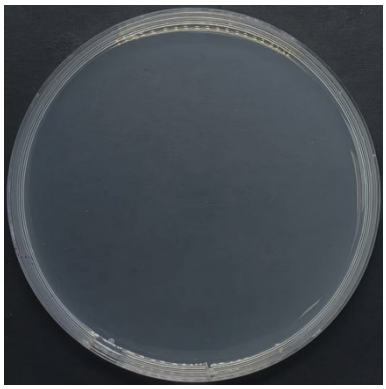

Figure S14. The growth of bacteria in evaporated water.

Table S1. The water evaporation rate and water evaporation conversion efficiency of different solar-thermal functional materials under 1.0 kW m^{-2} simulated solar irradiation.

System	Materials	Evaporation rate (kg m^{-2} h^{-1})	Evaporation conversion efficiency (%)	Ref.
Biomass material	WMT/H	1.360	76.28	This work
	FPyPP	1.220	76.61	1
	CL+AL	1.360	83.70	2
	SCW	1.525	78.44	3
	Rice straw	1.200	75.80	4
	SE/H	1.420	86.65	5

	PPy-bamboo	1.125	76.87	6

Table S2. The output voltage of different solar-thermal-electric systems under 1.0 kW m^{-2} simulated solar irradiation.

Materials	**Output voltage (mV)**	**Ref.**
WMT	93.40	This work
cotton/PPy	31.42	7
TPyP	60.00	8
TPA-SBTQ	106.00	9
4OCSPC	124.00	10
2TP-BBT	95.50	11
LPC-50 mg@CSL-5:5	108.40	12

1. C. Zhang, P. Xiao, F. Ni, L. Yan, Q. Liu, D. Zhang, J. Gu, W. Wang and T. Chen, *ACS Sustainable Chem. Eng.*, 2020, **8**, 5328.

2. Y. Lu, X. Wang, D. Fan, H. Yang, H. Xu, H. Min and X. Yang, *Sustainable Mater. Technol.*, 2020, **25**, e00180.

3. H. Hu, Y. Feng, X. Chen, L. Tian, Z. Yin, H. Wang, Y. Li, Y. Yang and Q. Sun, *J. Environ. Chem. Eng.*, 2024, **12**, 113419.

4. Q. Fang, T. Li, Z. Chen, H. Lin, P. Wang and F. Liu, *ACS Appl. Mater. Interfaces*, 2019, **11**, 10672.

5. S. Ao, Z. Chen, H. Chen, L. Zhang, Y. Wang, Y. Zhang, T. Jia, G. Xi and T. Peng, *J. Mater. Chem. A*, 2025, **13**, 15149.

6. P. Zhang, M. Xie, Y. Jin, C. Jin and Z. Wang, *ACS Appl. Polym. Mater.*, 2022, **4**, 2393.

7. H. Liu, X. Jin, Q. Xu, Y. Jin, X. Zhang and S.-L. Lv, *ACS Appl. Mater. Interfaces*, 2025, **17**, 36943.

8. Y. Zhang, H. Yan, X. Wang, Z. Zhang, F. Liu, S. Tu and X. Chen, *RSC Adv.*, 2022, **12**, 28997.

9. L. Wang, H. Wang, S. Yu, N. An, Y. Pan, J. Li, T. Jia, K. Wang and W. Huang, *Adv. Funct. Mater.*, 2024, **34**, 2315762.

10. X. Han, Z. Wang, M. Shen, J. Liu, Y. Lei, Z. Li, T. Jia and Y. Wang, *J. Mater. Chem. A*, 2021, **9**, 24452.

11. R. Zhang, N. Jin, T. Jia, L. Wang, J. Liu, M. Nan, S. Qi, S. Liu and Y. Pan, *J. Mater. Chem. A*, 2023, **11**, 15380-15388.

12. S. Chen, B. Yang, D. Yang, X. Qiu and D. Zheng, *ACS Nano*, 2025, **19**, 19681.